

Unveiling Invariances via Neural Network Pruning

Derek Xu¹, Yizhou Sun¹, Wei Wang¹

¹University of California, Los Angeles
derekxu@cs.ucla.edu, yzsun@cs.ucla.edu, weiwang@cs.ucla.edu

Abstract

Invariance describes transformations that do not alter data’s underlying semantics. Neural networks that preserve natural invariance capture good inductive biases and achieve superior performance. Hence, modern networks are handcrafted to handle well-known invariances (ex. translations). We propose a framework to learn novel network architectures that capture data-dependent invariances via pruning. Our learned architectures consistently outperform dense neural networks on both vision and tabular datasets in both efficiency and effectiveness. We demonstrate our framework on multiple deep learning models across 3 vision and 40 tabular datasets.

Introduction

Preserving invariance is a key property in successful neural network architectures. Invariance occurs when the semantics of data remains unchanged under a set of transformations (Bronstein et al. 2017). For example, an image of a cat can be translated, rotated, and scaled, without altering its underlying contents. Neural network architectures that represent data passed through invariant transformations with the same representation inherit a good inductive bias (Neyshabur 2020, 2017; Neyshabur, Tomioka, and Srebro 2014) and achieve superior performance (Zhang et al. 2021; Arpit et al. 2017).

Convolutional Neural Networks (CNNs) are one such example. CNNs achieve translation invariance by operating on local patches of data and weight sharing. Hence, early CNNs outperform large multilayer perceptrons (MLP) in computer vision (LeCun, Bengio, and Hinton 2015; LeCun et al. 1998). Recent computer vision works explore more general spatial invariances, such as rotation and scaling (Satorras, Hoogeboom, and Welling 2021; Deng et al. 2021; Delchevalerie et al. 2021; Sabour, Frosst, and Hinton 2017; Cohen and Welling 2016; Jaderberg et al. 2015; Qi et al. 2017; Jaderberg et al. 2015; Xu et al. 2014). Other geometric deep learning works extend CNNs to non-Euclidean data by considering additional data-type specific invariances, such as permutation invariance (Wu et al. 2020; Kipf and Welling 2016; Defferrard, Bresson, and Vandergheynst 2016).

Designing invariant neural networks requires substantial human effort: both to determine the set of invariant trans-

formations and to handcraft architectures that preserve said transformations. In addition to being labor-intensive, this approach has not yet succeeded for all data-types (Schäfl et al. 2022; Gorishniy, Rubachev, and Babenko 2022; Gorishniy et al. 2021; Huang et al. 2020). For example, designing neural architectures for tabular data is especially hard because the set of invariant tabular transformations is not clearly-defined. Thus, the state-of-the-art deep learning architecture on tabular data remains MLP (Kadra et al. 2021; Grinsztajn, Oyallon, and Varoquaux 2022).

Existing invariance learning methods operate at the data augmentation level (Immer et al. 2022; Quiroga et al. 2020; Benton et al. 2020; Cubuk et al. 2018), where a model is trained on sets of transformed samples rather than individual samples. This makes the network resilient to invariant transformations at test time. Contrastive learning (CL) is shown to be an effective means of incorporating invariance (Dangovski et al. 2021), and has seen success across various tasks (Chen, Xie, and He 2021; Zhu et al. 2021; You et al. 2020b; Jaiswal et al. 2020; Baevski et al. 2020; Chen et al. 2020), including tabular learning (Bahri et al. 2021). While these approaches train existing neural networks to capture new data-dependent invariances, the model architecture itself still suffers from a weak inductive bias.

In contrast, existing network pruning works found shallow MLPs can automatically be compressed into sparse subnetworks with good inductive bias by pruning the MLP itself (Neyshabur 2020). Combining pruning and invariance learning has largely been unsuccessful (Corti et al. 2022). Furthermore, pruning for invariance does not scale to deep MLPs, possibly due to issues in the lazy training regime (Tzen and Raginsky 2020; Chizat, Oyallon, and Bach 2019) where performance improves while weights magnitudes stay near static over training. Combining invariance learning with network pruning remains an open question.

We propose **Invariance Unveiling Neural Networks**, IUNET, a pruning framework that discovers invariance-preserving subnetworks from deep and dense supernetworks. We hypothesize pruning for invariances fails on deep networks due to the lazy training issue (Liu et al. 2023), where performance improvement decouples from weight magnitudes. We address this with a proactive initialization scheme (PIS), which prevents important weights from being accidentally pruned by assigning low magnitudes to major-

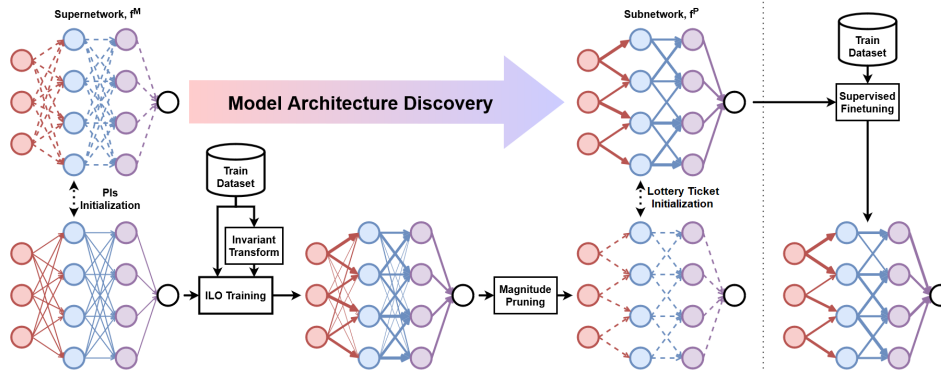


Figure 1: Overview for the IUNET Framework. The supernet, $f^P(\cdot, \theta_M)$, is initialized using PIS and trained on the ILO objective to obtain $\theta_M^{(T)}$. Magnitude-based pruning is used to get a new architecture $f^P = \mathcal{P}(\theta_M^{(T)})$. The new architecture, $f^P(\cdot, \theta_P)$, is initialized via lottery ticket reinitialization and finetuned with supervised maximum likelihood loss.

ity of weights. To capture useful invariances, we propose a novel invariance learning objective (ILO), that successfully combines CL with network pruning by regularizing CL with the supervised objective.

To the best of our knowledge, we are the first to automatically design deep architectures that incorporate invariance using pruning. We summarize our contributions below:

- Designing architectures from scratch is difficult when desired invariances are either unknown or hard to incorporate. We automatically discover an invariance-preserving subnetwork that outperforms an invariance-agnostic supernet on both computer vision and tabular data.
- Network pruning is used to compress models for mobile devices. Our approach consistently improves compression performance for existing vision and tabular models.
- Contrastive learning traditionally fails with network pruning. We are the first to successfully combine contrastive learning with network pruning by regularizing it in our invariance learning objective.
- In the lazy training regime, performance improves drastically while weight magnitudes stay relatively constant, hence weights important for downstream performance may not have large magnitudes and hence be falsely pruned. We provide a simple yet effective approach that encourages only important weights to have large magnitudes before the lazy training regime begins.

Related Work

Learning Invariances

Most invariant networks are handcrafted for spatial invariances (Dehmamy et al. 2021; Satorras, Hoogeboom, and Welling 2021; Deng et al. 2021; Qi et al. 2017; Vaswani et al. 2017; Cohen and Welling 2016; Kipf and Welling 2016; Jaderberg et al. 2015; LeCun et al. 1998). Learning approaches primarily involve data augmentation followed by ensembling. (Immer et al. 2022; Quiroga et al. 2020; Lorraine, Vicol, and Duvenaud 2020; Benton et al. 2020; Cubuk et al. 2018). Some works use meta-learning to do

parameter sharing in a given architecture (Zhou, Knowles, and Finn 2020; Kirsch et al. 2022). None of the aforementioned works generates architectures from scratch to improve the network’s inductive bias. The closest work is β -LASSO (Neysshabur 2020) which discovers shallow subnetworks with local connectivity through pruning for computer vision. Our work extends to deeper networks and explores the tabular data setting.

Neural Network Pruning

Neural network pruning compresses large supernetworks without hurting performance (Frankle and Carbin 2018; Louizos, Welling, and Kingma 2017). A pinnacle work is the Lottery Ticket Hypothesis (LTH) (Frankle and Carbin 2018; Liu et al. 2018; Blalock et al. 2020), where pruned networks can retain unpruned performance when reinitialized to the start of training and iteratively retrained. One-Shot Magnitude Pruning (OMP) studies how to prune the network only once (Blalock et al. 2020). Recent work (Liu et al. 2023) identifies the lazy training regime (Chizat, Oyalon, and Bach 2019) as a bottleneck for network pruning. Recent work (Corti et al. 2022) find contrastive learning does not work with netwprl pruning. Recent pruning policies improve efficiency by starting with a sparse network (Evcil et al. 2020). or performing data-agnostic Zero-Shot Pruning (Hoang et al. 2023; Wang, Zhang, and Grosse 2020; Lee et al. 2019). Interestingly, subnetworks rarely outperform the original supernet, which has been dubbed the “Jackpot” problem (Ma et al. 2021). In contrast to existing works, we successfully combine OMP with contrastive learning, alleviate the lazy learning issue, and outperform the original supernet.

Proposed Method: IUNET

Problem Setting

We study the classification task with inputs, $x \in \mathcal{X}$, class labels, $y \in \mathcal{Y}$, and hidden representations, $h \in \mathcal{H}$. Our neural network architecture, $f(x, \theta) : \mathcal{X} \rightarrow \mathcal{Y}$ is composed of an encoder, $f_E(\cdot, \theta) : \mathcal{X} \rightarrow \mathcal{H}$ and decoder, $f_D(\cdot, \theta) : \mathcal{H} \rightarrow \mathcal{Y}$,

Dataset	MLP _{vis}	OMP ^(MLP_{vis})	β -LASSO ^(MLP_{vis})	IUNET ^(MLP_{vis})
CIFAR10	59.266 \pm 0.050	59.668 \pm 0.171	59.349 \pm 0.174	64.847 \pm 0.121
CIFAR100	31.052 \pm 0.371	31.962 \pm 0.113	31.234 \pm 0.354	32.760 \pm 0.288
SVHN	84.463 \pm 0.393	85.626 \pm 0.026	84.597 \pm 0.399	89.357 \pm 0.156

Dataset	RESNET	OMP ^(RESNET)	β -LASSO ^(RESNET)	IUNET ^(RESNET)
CIFAR10	73.939 \pm 0.152	75.419 \pm 0.290	74.166 \pm 0.033	83.729 \pm 0.153
CIFAR100	42.794 \pm 0.133	44.014 \pm 0.163	42.830 \pm 0.412	53.099 \pm 0.243
SVHN	90.235 \pm 0.127	90.474 \pm 0.192	90.025 \pm 0.201	94.020 \pm 0.291

Table 1: Comparing different pruning approaches to improve the inductive bias of MLP_{vis} and RESNET on computer vision datasets. Notice, IUNET performs substantially better than existing pruning-based methods by discovering novel architectures that better capture the inductive bias. IUNET flexibly boosts performance of off-the-shelf models.

Dataset	IUNET ^(MLP_{vis})	CNN
CIFAR10	64.847 \pm 0.121	75.850 \pm 0.788
CIFAR100	32.760 \pm 0.288	41.634 \pm 0.402
SVHN	89.357 \pm 0.156	91.892 \pm 0.411

Table 2: Comparing the pruned IUNET^(MLP_{vis}) model to an equivalent CNN. Although IUNET^(MLP_{vis}) cannot outperform CNN, it bridges the gap between MLP and CNN architectures without any human design intervention.

Dataset	$g(\cdot)$	MLP _{vis}	IUNET ^(MLP_{vis})
CIFAR10	resize.	44.096 \pm 0.434	97.349 \pm 4.590
	horiz.	80.485 \pm 0.504	99.413 \pm 1.016
	color.	56.075 \pm 0.433	98.233 \pm 3.060
	grayscale.	81.932 \pm 0.233	99.077 \pm 1.598

Dataset	$g(\cdot)$	MLP _{TAB}	IUNET ^(MLP_{TAB})
mfeat.	feat.	46.093 \pm 1.353	51.649 \pm 4.282

Table 3: Comparing the consistency metric (%) of the untrained supernetwork, MLP_{vis} and MLP_{TAB}, against IUNET’s pruned subnetwork under different invariant transforms, $g(\cdot)$. IUNET preserves invariances better.

where $\theta \in \Theta$ are the weights and $f = f_{\mathcal{E}} \circ f_{\mathcal{D}}$. In the context of training, we denote the weights after $0 < t < T$ iterations of stochastic gradient descent as $\theta^{(t)}$.

First, we define our notion of invariance. Given a set of invariant transformations, \mathcal{S} , we wish to discover a neural network architecture $f^*(x, \theta)$, such that all invariant input transformations map to the same representation, shown in Equation 1. We highlight our task focuses on the discovery of novel architectures, $f^*(\cdot, \theta)$, not weights, θ , because good architectures improves the inductive bias (Neyshabur 2017).

$$f_{\mathcal{E}}^*(x, \theta) = f_{\mathcal{E}}^*(g(x), \theta), \forall g \in \mathcal{S}, \forall \theta \in \Theta. \quad (1)$$

Framework

We accomplish this by first training a dense supernetwork, $f^M(\cdot, \theta_M)$, with enough representational capacity to capture the desired invariance properties, as shown in Equation 2. A natural choice for $f^M(\cdot, \theta_M)$ is a deep MLP, which is a universal approximator (Cybenko 1989).

$$\exists \theta_M^* \in \Theta_M : f_{\mathcal{E}}^M(x, \theta_M^*) = f_{\mathcal{E}}^M(g(x), \theta_M^*), \forall g \in \mathcal{S}. \quad (2)$$

Next, we initialize the supernetwork’s weights, $\theta_M^{(0)}$, using our Proactive Initialization Scheme, PIS, and train the supernetwork with our Invariance Learning Objective, ILO, to obtain $\theta_M^{(T)}$. We discuss both PIS’s and ILO’s details in following sections.

We construct our new untrained subnetwork, $f^P(\cdot, \theta_P^{(0)})$, from the trained supernetwork, $f^M(\cdot, \theta_M^{(T)})$, where the subnetwork contains a fraction of the supernetwork’s weights, $\theta_P^{(0)} \subset \theta_M^{(T)}$ and $|\theta_P^{(0)}| \ll |\theta_M^{(T)}|$, and is architecturally different from the supernetwork, $f^P(\cdot, \cdot) \neq f^M(\cdot, \cdot)$. For this step, we adopt standard One-shot Magnitude-based Pruning (OMP), where the smallest magnitude weights and their connections in the supernetwork architecture are dropped. We adopt OMP because of its success in neural network pruning (Frankle and Carbin 2018; Blalock et al. 2020). We represent this step as an operator mapping supernetwork weights into subnetwork architectures $\mathcal{P} : \Theta_M \rightarrow \mathcal{F}_P$, where \mathcal{F}_P denotes the space of subnetwork architectures.

We hypothesize the trained subnetwork, $f^P(\cdot, \theta_P^{(T)})$, can outperform the trained original supernetwork, $f^M(\cdot, \theta_M^{(T)})$, if it learns to capture the right invariances and hence achieving a better inductive bias. The ideal subnetwork, $f^{P*}(\cdot, \theta_{P*})$, could capture invariances without training, as shown in Equation 3.

$$f_{\mathcal{E}}^{P*}(x, \theta_{P*}) = f_{\mathcal{E}}^{P*}(g(x), \theta_{P*}), \forall g \in \mathcal{S}, \forall \theta_{P*} \in \Theta_{P*} \quad (3)$$

Finally, we re-initialize the subnetwork’s weights, $\theta_P^{(0)}$, using the Lottery Ticket Re-initialization scheme (Frankle and Carbin 2018) then finetune the subnetwork with maximum likelihood loss to obtain $\theta_P^{(T)}$. We call this framework, including the ILO objective and PIS initialization scheme, IUNET¹, as shown in Figure 1

¹IUNET prunes an ineffective supernetwork into an efficient effective subnetwork. OMP prunes an inefficient effective supernetwork into an efficient but slightly less effective subnetwork.

Invariance Learning Objective: ILO The goal of supernet training is to create a subnetwork, $f^P(\cdot, \theta_P^{(0)})$, within the supernet, $f^M(\cdot, \theta_M^{(T)})$, such that:

1. $\mathcal{P}(\theta_M^{(T)})$ achieves superior performance on the classification task after finetuning.
2. $\mathcal{P}(\theta_M^{(T)})$ captures desirable invariance properties as given by Equation 3.
3. $\theta_P^{(0)}$ has higher weight values than $\theta_M^{(T)} \setminus \theta_P^{(0)}$.

Because subnetworks pruned from randomly initialized weights, $\mathcal{P}(\theta_M^{(0)})$, are poor, they include harmful inductive biases that hinders training. Thus, we optimize the trained supernet, $f^M(\cdot, \theta_M^{(T)})$, on goals (1) and (2) as a surrogate training objective. Goal (3) is handled by PIS, described in the next section.

To achieve (1), we maximize the log likelihood of the data. To achieve (2), we minimize a distance metric, $\phi(\cdot, \cdot)$, between representations of inputs under invariant perturbations and maximize the metric between different input samples, given by Equation 9. We prove this is equivalent to Supervised Contrastive Learning (SCL) in the Supplementary Material. Hence, (2) can be achieved through SCL.

$$\theta_M^* = \underset{\theta_M}{\operatorname{argmax}} \mathbb{E}_{\substack{x_i \\ x_j \sim \mathcal{X} \\ g \sim \mathcal{S}}} \left[\frac{\phi(f_{\mathcal{E}}^M(x_i, \theta_M), f_{\mathcal{E}}^M(x_j, \theta_M))}{\phi(f_{\mathcal{E}}^M(x_i, \theta_M), f_{\mathcal{E}}^M(g(x_i), \theta_M))} \right] \quad (4)$$

Our final Invariance Learning Objective (ILO) loss function combines these two ideas as shown in Equation 6, where \mathcal{L}_{SUP} is standard maximum likelihood loss, \mathcal{L}_{NCE} is a contrastive loss (described in Appendix), D_{tr} is a labelled training dataset of (x, y) pairs, and λ is a hyperparameter.

$$\mathcal{L}(\theta_M; \mathcal{S}) = \mathbb{E}_{x, y \sim D_{tr}} [\mathcal{L}_{SUP}(x, y, \theta_M) + \lambda \mathcal{L}_{NCE}(x, y, \theta_M; \mathcal{S})] \quad (5)$$

Both loss components are crucial to IUNET. With just \mathcal{L}_{NCE} , the supernet will overfit the contrastive objective (Corti et al. 2022; Pasad, Chou, and Livescu 2021), causing weights critical for finetuning the supervised objective to be pruned. With just \mathcal{L}_{SUP} , the architecture is not explicitly optimized to capture desired invariances.

Proactive Initialization Scheme: PIS Deep neural networks often enter the lazy training regime (Chizat, Oyalon, and Bach 2019; Liu et al. 2023), where the loss steadily decreases while weights barely change. This is particularly harmful to neural networks pruning (Liu et al. 2023), especially when low-magnitude weights contribute to decreasing the loss and hence should not be pruned.

We propose a simple solution by scaling the weight initialization by a small multiplier, κ . We find this alleviates the aforementioned issue by forcing the model to assign large values only to important weights prior to lazy training. Because lazy training is only an issue for pruning, we only apply κ -scaling to the pre-pruning training stage, not the

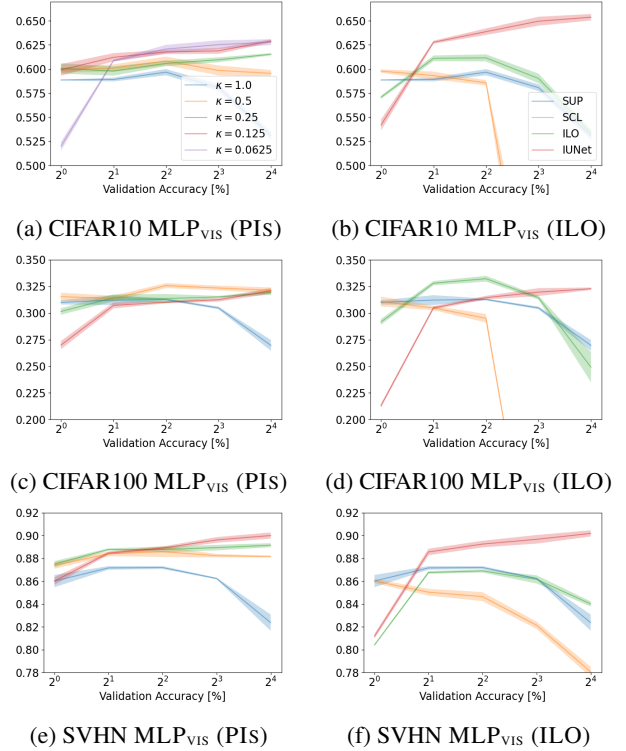


Figure 2: Effect of PIS and ILO on pruned models. The y-axis is the validation accuracy (%) and x-axis is the compression ratio. PIS experiments only alter the supernet’s initialization. $\kappa = 1.0$ means normal initialization. ILO experiments only alter the training objective during supernet training. After supernet training, subnetworks are pruned under different compression ratios, then finetuned. Validation accuracy of trained pruned models are reported.

fine-tuning stage. This is done by scaling the initial weights $\theta_M^{(0)} = \kappa \theta_{M^i}^{(0)}$, where $\theta_{M^i}^{(0)}$ follows the Kaiming (He et al. 2015) or Glorot (Glorot and Bengio 2010) initialization.

Experiment Setup

Datasets

IUNET is evaluated on *image* and *tabular* classification ²:

- **Vision:** Experiments are run on CIFAR10, CIFAR100, and SVHN (Krizhevsky, Hinton et al. 2009; Netzer et al. 2011), following baseline work (Neyshabur 2020)³.
- **Tabular:** Experiments are run on 40 tabular datasets from a benchmark paper (Kadra et al. 2021), covering a diverse range of problems. The datasets were collected from OpenML (Gijsbers et al. 2019), UCI (Asuncion and Newman 2007), and Kaggle.

²More details are provided in the Supplementary.

³While SMC benchmark (Liu et al. 2023) is open-sourced, it is undergoing code clean-up at the time of submission.

Dataset	MLP _{VIS}	IUNET ^(MLP_{VIS}) _{NO-PRUNE}	IUNET ^(MLP_{VIS}) _{NO-ILO}	IUNET ^(MLP_{VIS}) _{NO-PIS}	IUNET ^(MLP_{VIS})
CIFAR10	59.266 ± 0.050	54.622 ± 0.378	62.662 ± 0.169	60.875 ± 0.292	83.729 ± 0.153
CIFAR100	31.052 ± 0.371	20.332 ± 0.065	32.242 ± 0.321	32.747 ± 0.346	53.099 ± 0.243
SVHN	84.463 ± 0.393	78.427 ± 0.683	88.870 ± 0.139	85.247 ± 0.071	94.020 ± 0.291

Dataset	MLP _{TAB}	IUNET ^(MLP_{TAB}) _{NO-PRUNE}	IUNET ^(MLP_{TAB}) _{NO-ILO}	IUNET ^(MLP_{TAB}) _{NO-PIS}	IUNET ^(MLP_{TAB})
arrhythmia	67.086 ± 2.755	56.780 ± 6.406	71.385 ± 6.427	78.675 ± 7.078	74.138 ± 2.769
mfeat.	98.169 ± 0.297	97.528 ± 0.400	98.471 ± 0.344	98.339 ± 0.203	98.176 ± 0.121
vehicle	80.427 ± 1.829	80.427 ± 1.806	81.411 ± 0.386	80.928 ± 0.861	81.805 ± 2.065
kc1	80.762 ± 1.292	84.597 ± 0.000	82.456 ± 1.850	84.597 ± 0.000	84.597 ± 0.000

Table 4: Ablation Study on vision and tabular datasets.

Model Setup

IUNET is compared against One-shot Magnitude Pruning (OMP) (Blalock et al. 2020), and β -LASSO pruning (Neyshabur 2020) on all datasets. We denote the supernet used by each pruning method with a superscript. Unless otherwise specified, models are trained via maximum likelihood. In addition, we compare against the following dataset-specific supernetworks (MLP_{VIS}, MLP_{TAB}, RESNET) and models:

- **Vision:** We consider RESNET (He et al. 2016), MLP_{VIS}, a MLP that contains a CNN subnetwork (Neyshabur 2020), and the aforementioned CNN subnetwork.
- **Tabular:** We consider MLP_{TAB}, a 9-layer MLP with hidden dimension 512 (Kadra et al. 2021), XGB (Chen and Guestrin 2016), TABN (Arik and Pfister 2021), a handcrafted tabular deep learning architecture, and MLP_{TAB+C} (Kadra et al. 2021), the state-of-the-art MLP, which was heavily tuned from a cocktail of regularization techniques.

Considered Invariances

Because contrastive learning is successful on both vision and tabular datasets, our invariant transformations, \mathcal{S} , come from existing works. For computer vision, SimCLR (Chen et al. 2020) transformations are used: (1) resize crops, (2) horizontal flips, (3) color jitter, and (4) random grayscale. For tabular learning, SCARF (Bahri et al. 2021) transformations are used: (5) randomly corrupting features by drawing the corrupted versions from its empirical marginal distribution.

Results

On Inductive Bias

In this section, we compare the effectiveness of the trained subnetwork discovered by IUNET, $f^P(\cdot, \theta_P^{(T)})$, against the trained supernet, $f^M(\cdot, \theta_M^{(T)})$. As seen in Tables 1 and 5, the pruned subnetwork outperforms the original supernet, even though the supernet has more representational capacity. This supports our claim that IUNET prunes subnetwork architectures with better inductive biases than the supernet. Importantly, IUNET substantially improves upon existing pruning baselines by explicitly including invariances via ILO and alleviating the lazy learning issue (Liu et al. 2023) via PIS.

On *vision* datasets: As seen in Figure 1, IUNET is a general and flexible framework that improves the inductive bias of not only models like MLP_{VIS} but also specialized architectures like RESNET. As seen in Figure 2, IUNET bridges the gap between MLPs and CNNs. Unlike previous work (Tolstikhin et al. 2021), IUNET does this in an entirely automated procedure. While CNN outperforms IUNET^(MLP_{VIS}), we can also apply IUNET to specialized networks, IUNET^(RESNET), which achieves the best overall performance. Figures 1 and 2 show IUNET is a useful tool for injecting inductive bias into arbitrary neural architectures.

On *tabular* datasets: As seen in Figure 5, the subnetworks derived from MLPs outperform both the original MLP_{TAB} and hand-crafted architectures: TABN and XGB. Unlike vision, how to encode invariances for tabular data is highly nontrivial, making IUNET particularly effective. Note, although IUNET performs competitively against MLP_{TAB+C}, they are orthogonal approaches. MLP_{TAB+C} focuses on tuning regularization hyperparameters during finetuning, whereas IUNET improves the model architecture. Note, IUNET^(MLP_{TAB}) did not use the optimal hyperparameters found by MLP_{TAB+C} (Kadra et al. 2021).

Ablation Study

To study the effectiveness of (1) pruning, (2) PIS, and (3) ILO, each one is removed from the optimal model. As seen in Table 4, each is crucial to IUNET. Pruning is necessary to encode the inductive bias into the subnetwork’s neural architecture. PIS and ILO improves the pruning policy by ensuring weights crucial to finetuning and capturing invariance are not pruned. Notice, without pruning, IUNET_{NO-PRUNE} performs worse than the original supernet. This highlights an important notion that PIS aims to improve the pruning policy, not the unpruned performance. By sacrificing unpruned performance, PIS ensures important weights are not falsely pruned. PIS is less effective on tabular datasets where the false pruning issue seems less severe. Combining pruning, ILO, and PIS, IUNET most consistently achieves the best performance.

Effects of Pruning

To further study the effects of pruning, we plot how performance changes over different compression ratios. Figure 2 clearly identifies how PIS and ILO substantially improves

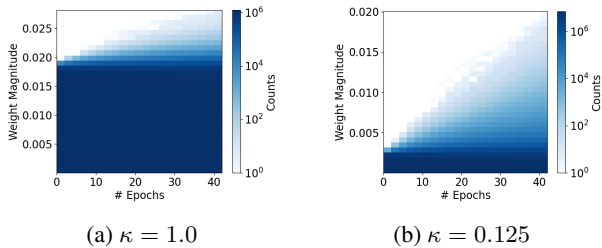


Figure 3: Histogram of weight magnitudes, $|\theta_M^{(t)}|$, plotted over each epoch under different κ initialization settings. $\kappa = 1.0$ means normal initialization. Results shown for MLP_{VIS} on the CIFAR10 dataset.

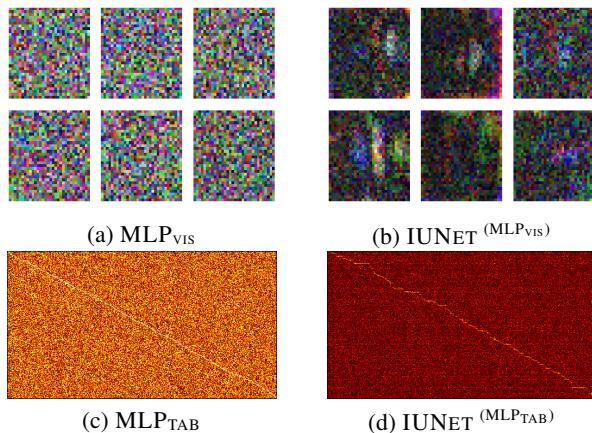


Figure 4: Visualization of weight magnitudes, $|\theta_M^{(T)}|$, trained with different policies. The top row was trained on CIFAR10 and shows the magnitude of each RGB pixel for 6 output logits. The bottom row was trained on arrhythmia and shows the weight matrix of the 1st layer with 280 input and 512 output dimensions. Lighter color means larger magnitude.

upon existing pruning policies. First, our results support existing findings that (1) OMP does not produce subnetworks that substantially outperform the supernet (Blalock et al. 2020) and (2) while unpruned models trained with SCL can outperform supervised ones, pruned models trained with SCL perform substantially worse (Corti et al. 2022). PIS flips the trend from (1) by slightly sacrificing unpruned performance, due to poorer initialization, IUNET discovers pruned models with better inductive biases, which improves downstream performance. ILO fixes the poor performance of SCL in (2) by preserving information pathways for both invariance and max likelihood over training. We highlight both these findings are significant among the network pruning community. Finally, Figure 2 confirms IUNET achieves the best performance by combining both PIS and ILO.

In addition to being more effective than the supernet, $f^M(\cdot, \theta_M^{(T)})$, the pruned network, $f^P(\cdot, \theta_P^{(T)})$, is also more efficient. Figure 2 shows IUNET can reach 8-16 \times compression while still keeping superior performance.

Effect of Proactive Initialization

To further study the role of PIS, the histogram of weight magnitudes is monitored over the course of training. As shown in Figure 5, under the standard OMP pruning setup, the histogram changes little over the course of training, which supports the lazy training hypothesis (Liu et al. 2023) where performance rapidly improves, while weight magnitudes change very little, decoupling each weight’s importance from its magnitude.

With PIS, only important weights grow over the course of training, while most weights remain near zero, barely affecting the output activations of each layer. This phenomenon alleviates the lazy training problem by ensuring (1) pruning safety, as pruned weights are near zero prior which have minimal affect on layer activations, and (2) importance-magnitude coupling, as structurally important connections must grow to affect the output of the layer.

On Invariance Consistency

To further study whether particular invariances are learned, we compute the consistency metric (Singla et al. 2021), which measure the percentage of samples whose predicted label would flip when an invariant transformation is applied to the input. As seen in Table 3, the subnetwork found by IUNET, $f^P(\cdot, \theta_P^{(0)})$, is able to preserve invariances specified in ILO much better than the supernet, $f^M(\cdot, \theta_M^{(0)})$. This shows IUNET indeed captures desirable invariances.

On Weight Visualization

We visualize the supernet weights, $\theta_M^{(T)}$, when trained with IUNET compared to standard maximum likelihood (MLP) to determine what structures preserve invariance.

On *vision* datasets: As seen in Figure 6, IUNET learns more locally connected structures, which improves translation invariance. Prior work (Neyshabur 2020) found network structure (as opposed to inductive bias) to be the limiting factor for encoding CNN inductive biases into MLPs, which IUNET successfully replicates.

On *tabular* datasets: As seen in Figure 6, IUNET weights focus more on singular features. This preserves invariance over random feature corruption, as the absence of some tabular features does not greatly alter output activations of most neurons. This structure can also be likened to tree ensembles (Grinsztajn, Oyallon, and Varoquaux 2022), whose leaves split individual features rather than all features.

Conclusion

In this work, we study the viability of network pruning for discovering invariant-preserving architectures. Under the computer vision setting, IUNET bridges the gap between deep MLPs and deep CNNs, and reliably boosts RESNET performance. Under the tabular setting, IUNET reliably boosts performance of existing MLPs, comparable to applying the state-of-the-art regularization cocktails. Our proposed novelties, ILO and PIS, flexibly improves existing OMP pruning policies by both successfully integrating contrastive learning and alleviating lazy training. Thus, IUNET effectively uses pruning to tackle invariance learning.

Dataset	MLP _{TAB}	OMP (MLP _{TAB})	β -LASSO (MLP _{TAB})	IUNET (MLP _{TAB})	XGB	TABN	MLP _{TAB+C}
credit-g	70.000	70.000 \pm 0.000	67.205 \pm 0.718	63.166 \pm 0.000	68.929	61.190	74.643
anneal	99.490	99.691 \pm 0.234	99.634 \pm 0.518	99.712 \pm 0.101	85.416	84.248	89.270
kr-vs-kp	99.158	99.062 \pm 0.142	99.049 \pm 0.097	99.151 \pm 0.064	99.850	93.250	99.850
arrhythmia	67.086	55.483 \pm 5.701	67.719 \pm 3.483	74.138 \pm 2.769	48.779	43.562	61.461
mfeat.	98.169	97.959 \pm 0.278	97.204 \pm 0.620	98.176 \pm 0.121	98.000	97.250	98.000
vehicle	80.427	81.115 \pm 2.214	80.611 \pm 1.244	81.805 \pm 2.065	74.973	79.654	82.576
kc1	80.762	84.597 \pm 0.000	83.587 \pm 1.010	84.597 \pm 0.000	66.846	52.517	74.381
adult	81.968	82.212 \pm 0.582	82.323 \pm 0.424	78.249 \pm 3.085	79.824	77.155	82.443
walking.	58.466	60.033 \pm 0.112	58.049 \pm 0.309	59.789 \pm 0.456	61.616	56.801	63.923
phoneme	84.213	86.733 \pm 0.194	84.850 \pm 1.548	87.284 \pm 0.436	87.972	86.824	86.619
skin-seg.	99.869	99.866 \pm 0.016	99.851 \pm 0.015	99.876 \pm 0.006	99.968	99.961	99.953
ldpa	66.590	68.458 \pm 0.140	62.362 \pm 4.605	64.816 \pm 4.535	99.008	54.815	68.107
nomao	95.776	95.682 \pm 0.046	95.756 \pm 0.074	95.703 \pm 0.110	96.872	95.425	96.826
cnae	94.080	92.742 \pm 0.404	94.808 \pm 0.254	96.075 \pm 0.242	94.907	89.352	95.833
blood.	68.965	61.841 \pm 10.012	65.126 \pm 20.792	70.375 \pm 5.255	62.281	64.327	67.617
bank.	88.300	88.300 \pm 0.000	86.923 \pm 1.948	88.300 \pm 0.000	72.658	70.639	85.993
connect.	72.111	72.016 \pm 0.112	72.400 \pm 0.214	74.475 \pm 0.445	72.374	72.045	80.073
shuttle	99.709	93.791 \pm 3.094	99.687 \pm 0.027	93.735 \pm 2.303	98.563	88.017	99.948
higgs	72.192	72.668 \pm 0.039	72.263 \pm 0.149	73.215 \pm 0.384	72.944	72.036	73.546
australian	82.153	83.942 \pm 1.578	81.667 \pm 1.572	82.562 \pm 1.927	89.717	85.278	87.088
car	99.966	100.000 \pm 0.000	100.000 \pm 0.000	99.859 \pm 0.200	92.376	98.701	99.587
segment	91.504	91.603 \pm 0.508	91.317 \pm 0.074	91.563 \pm 0.000	93.723	91.775	93.723
fashion.	91.139	90.784 \pm 0.158	90.864 \pm 0.090	90.817 \pm 0.040	91.243	89.793	91.950
jungle.	86.998	92.071 \pm 0.420	87.400 \pm 0.489	95.130 \pm 0.807	87.325	73.425	97.471
numerai	51.621	51.443 \pm 0.370	51.905 \pm 0.299	51.839 \pm 0.067	52.363	51.599	52.668
devnagari	97.550	97.573 \pm 0.031	97.549 \pm 0.014	97.517 \pm 0.014	93.310	94.179	98.370
helena	29.342	28.459 \pm 0.531	29.834 \pm 0.354	29.884 \pm 0.991	21.994	19.032	27.701
jannis	68.647	66.302 \pm 3.887	69.302 \pm 0.248	69.998 \pm 1.232	55.225	56.214	65.287
volkert	70.066	68.781 \pm 0.045	69.655 \pm 0.189	70.104 \pm 0.215	64.170	59.409	71.667
miniboone	86.539	87.575 \pm 0.855	87.751 \pm 0.398	81.226 \pm 6.569	94.024	62.173	94.015
apsfailure	97.041	98.191 \pm 0.000	98.048 \pm 0.203	98.191 \pm 0.000	88.825	51.444	92.535
christine	70.295	69.819 \pm 0.462	70.275 \pm 1.045	69.065 \pm 1.225	74.815	69.649	74.262
dilbert	98.494	98.738 \pm 0.029	98.522 \pm 0.084	98.540 \pm 0.023	99.106	97.608	99.049
fabert	65.540	64.709 \pm 0.293	66.681 \pm 0.208	65.695 \pm 0.065	70.098	62.277	69.183
jasmine	78.691	80.139 \pm 1.978	78.415 \pm 1.731	80.864 \pm 0.374	80.546	76.690	79.217
sylvine	92.660	92.650 \pm 0.267	92.593 \pm 0.368	93.369 \pm 0.833	95.509	83.595	94.045
dionis	93.920	93.687 \pm 0.059	93.943 \pm 0.037	93.586 \pm 0.021	91.222	83.960	94.010
aloi	96.546	96.376 \pm 0.069	96.562 \pm 0.087	95.341 \pm 0.194	95.338	93.589	97.175
ccfraud	97.554	97.748 \pm 1.622	96.626 \pm 3.202	98.797 \pm 1.031	90.303	85.705	92.531
clickpred.	82.175	83.206 \pm 0.000	82.307 \pm 0.500	85.270 \pm 1.275	58.361	50.163	64.280
#Best	1	4	1	13	12	0	16

Table 5: Comparing IUNET against trees (XGB), handcrafted models (TABN), and state-of-the-art regularized MLPs (MLP_{TAB+C}). The last row denotes the number of datasets where the model achieves the best performance. Note, our method does not tune the optimal regularization settings for each dataset making it more efficient. Our pruned model is also more compressed than the original network. Note, we outperform both MLP_{TAB} and TABN on most datasets. While IUNET performs similarly to MLP_{TAB+C}, it does not require costly hyperparameter tuning, and can be applied on top of the optimal settings found by MLP_{TAB+C}.

Additional Related Work

Tabular Machine Learning

Tabular data is a difficult regime for deep learning, where deep learning models struggle against decision tree approaches. Early methods use forests, ensembling, and boosting (Shwartz-Ziv and Armon 2022; Borisov et al. 2022; Chen and Guestrin 2016). Later, researchers handcrafted new deep architectures that mimic trees (Popov, Morozov, and Babenko 2019; Arik and Pfister 2021). Yet, when evaluated on large datasets, these approaches are still beaten by XGB (Chen and Guestrin 2016; Grinsztajn, Oyallon, and Varoquaux 2022). Recent work found MLPs with heavy regularization tuning (Kadra et al. 2021) can outperform decision tree approaches, though this conclusion does not hold on small tabular datasets (Joseph and Raj 2022). To specially tackle the small data regime, Bayesian learning and Hopfield networks are combined with MLPs (Hollmann et al. 2022; Schäfl et al. 2022). There are also work on tabular transformers (Huang et al. 2020), though said approaches require much more training data. Without regularization, tree based models still outperform MLPs due to a better inductive bias and resilience to noise (Grinsztajn, Oyallon, and Varoquaux 2022). To the best of our knowledge, the state-of-the-art on general tabular datasets remain heavily regularized MLPs (MLP_{TAB+C}) (Kadra et al. 2021). We aim to further boost regularized MLP performance by discovering model architectures that capture good invariances from tabular data.

Contrastive Learning

Contrastive learning, initially proposed for metric learning (Chopra, Hadsell, and LeCun 2005; Schroff, Kalenichenko, and Philbin 2015; Oh Song et al. 2016), trains a model to learn shared features among images of the same type (Jaiswal et al. 2020). It has been widely used in self-supervised pretraining (Chen et al. 2020; Chen, Xie, and He 2021), where dataset augmentation is crucial. Although contrastive learning was originally proposed for images, it has also shown promising results in graph data (Zhu et al. 2021; You et al. 2020b), speech data (Baevski et al. 2020), and tabular data (Bahri et al. 2021). Previous study has showed that speech transformers tend to overfit the contrastive loss in deeper layers, suggesting that removing later layers can be beneficial during finetuning (Pasad, Chou, and Livescu 2021). While contrastive learning performs well pretraining unpruned models, its vanilla formulation performs poorly after network pruning (Corti et al. 2022). In this work, we establish a connection between contrastive learning and invariance learning and observe that pruned contrastive models fail because of overfitting.

Neural Architecture Search

Neural Architecture Search (NAS) explores large superarchitectures by leveraging smaller block architectures (Wan et al. 2020; Pham et al. 2018; Zoph et al. 2018; Luo et al. 2018; Liu, Simonyan, and Yang 2018). These block architectures are typically small convolutional neural networks (CNNs) or MLPs. The key idea behind NAS is to utilize these blocks (Pham et al. 2018; Zoph et al. 2018) to

capture desired invariance properties for downstream tasks. Prior works (You et al. 2020a; Xie et al. 2019) have analyzed randomly selected intra- and inter-block structures and observed performance differences between said structures. However, these work did not propose a method for discovering block architectures directly from data. Our work aims to address this gap by focusing on discovering the architecture within NAS blocks. This approach has the potential to enable NAS in diverse domains, expanding its applicability beyond the current scope.

Loss Function Details

We provide a more detailed description of our loss function in this section. Following notation from the main paper, we repeat the ILO loss function in Equation 6 below:

$$\mathcal{L}(\theta; \mathcal{S}) = \mathbb{E}_{x,y \sim D_{train}} [\mathcal{L}_{SUP}(x, y, \theta) + \lambda \mathcal{L}_{NCE}(x, y, \theta; \mathcal{S})] \quad (6)$$

To better explain our loss functions, we introduce some new notations. First, we denote the decoder output probability function over classes, \mathcal{Y} , as $\tilde{p}_{\theta_D} : \mathcal{H} \rightarrow [0, 1]^{|\mathcal{Y}|}$, where $f_D = \text{argmax} \circ \tilde{p}_{\theta_D}$. We denote the model output probability function by combining \tilde{p}_{θ_D} with the encoder as follows: $p_\theta = \tilde{p}_{\theta_D} \circ f_\mathcal{E}$. We introduce an integer mapping from classes \mathcal{Y} as $\mathcal{I} : \mathcal{Y} \rightarrow \{0, 1, 2, \dots, |\mathcal{Y}| - 1\}$.

We show the maximum likelihood loss, \mathcal{L}_{SUP} , in Equation 7 below.

$$\mathcal{L}_{SUP}(x, y, \theta) = -\log(p_\theta(x, \theta)_{\mathcal{I}(y)}) \quad (7)$$

We show the supervised contrastive loss, \mathcal{L}_{NCE} , in Equation 8 below. Following SimCLR (Chen et al. 2020), we assume that the intermediary representations are d -dimensional embeddings, $\mathcal{H} = \mathbb{R}^d$, and use the cosine similarity as our similarity function, $\psi^{(cos)} : \mathbb{R}^d \times \mathbb{R}^d \rightarrow \mathbb{R}$.

$$\mathcal{L}_{NCE}(x, y, \theta; \mathcal{S}) = \mathbb{E}_{g \sim \mathcal{S}} \left[-\log \left(\frac{\exp \left(\psi^{(cos)} \left(\frac{f_\mathcal{E}(x, \theta)}{f_\mathcal{E}(g(x), \theta)} \right) \right)}{\sum_{\substack{x', y' \sim D_{tr} \\ y' \neq y}} \exp \left(\psi^{(cos)} \left(\frac{f_\mathcal{E}(x', \theta)}{f_\mathcal{E}(g(x'), \theta)} \right) \right)} \right) \right] \quad (8)$$

Surrogate Objective

We aim to learn invariance-preserving network architectures from the data. In our framework, this involves optimizing our invariance objective, which we repeat in Equation 9. We now prove that by minimizing the supervised contrastive loss in Equation 8 we equivalently maximize the invariance objective, outlined below.

$$\theta^* = \underset{\theta}{\text{argmax}} \mathbb{E}_{\substack{x_i, x_j \sim \mathcal{X} \\ g \sim \mathcal{S}}} \left[\frac{\phi(f_\mathcal{E}^M(x_i, \theta), f_\mathcal{E}^M(x_j, \theta))}{\phi(f_\mathcal{E}^M(x_i, \theta), f_\mathcal{E}^M(g(x_i), \theta))} \right] \quad (9)$$

We convert the distance metric ϕ into similarity metric ψ .

$$\begin{aligned}
\theta^* &= \underset{\theta}{\operatorname{argmax}} \mathbb{E}_{\substack{x_i, x_j \sim \mathcal{X} \\ g \sim \mathcal{S}}} \left[\frac{\psi(f_{\mathcal{E}}^M(x_i, \theta), f_{\mathcal{E}}^M(g(x_i), \theta))}{\psi(f_{\mathcal{E}}^M(x_i, \theta), f_{\mathcal{E}}^M(x_j, \theta))} \right] \\
&= \underset{\theta}{\operatorname{argmin}} \mathbb{E}_{\substack{x_i, x_j \sim \mathcal{X} \\ g \sim \mathcal{S}}} \left[\frac{-\psi(f_{\mathcal{E}}^M(x_i, \theta), f_{\mathcal{E}}^M(g(x_i), \theta))}{\psi(f_{\mathcal{E}}^M(x_i, \theta), f_{\mathcal{E}}^M(x_j, \theta))} \right] \\
&= \underset{\theta}{\operatorname{argmin}} \mathbb{E}_{\substack{x \sim \mathcal{X} \\ g \sim \mathcal{S}}} \left[\frac{-\psi(f_{\mathcal{E}}^M(x, \theta), f_{\mathcal{E}}^M(g(x), \theta))}{\sum_{\substack{x' \sim \mathcal{X} \\ x' \neq x}} \psi(f_{\mathcal{E}}^M(x, \theta), f_{\mathcal{E}}^M(g(x'), \theta))} \right] \\
&= \underset{\theta}{\operatorname{argmin}} \mathbb{E}_{\substack{x, y \sim D_{\text{tr}} \\ g \sim \mathcal{S}}} \left[\frac{-\psi\left(\frac{f_{\mathcal{E}}^M(x, \theta)}{f_{\mathcal{E}}^M(g(x), \theta)}\right)}{\sum_{\substack{x', y' \sim D_{\text{tr}} \\ y' \neq y}} \psi\left(\frac{f_{\mathcal{E}}^M(x, \theta)}{f_{\mathcal{E}}^M(g(x'), \theta)}\right)} \right] \\
&= \underset{\theta}{\operatorname{argmin}} \mathbb{E}_{\substack{x, y \sim D_{\text{tr}} \\ g \sim \mathcal{S}}} \left[-\log \left(\frac{\psi\left(\frac{f_{\mathcal{E}}^M(x, \theta)}{f_{\mathcal{E}}^M(g(x), \theta)}\right)}{\sum_{\substack{x', y' \sim D_{\text{tr}} \\ y' \neq y}} \psi\left(\frac{f_{\mathcal{E}}^M(x, \theta)}{f_{\mathcal{E}}^M(g(x'), \theta)}\right)} \right) \right] \tag{10}
\end{aligned}$$

We set the similarity metric, ψ , to be the same as our contrastive loss: $\psi(\cdot) = \exp(\psi^{\text{(cos)}}(\cdot))$.

$$\theta^* = \underset{\theta}{\operatorname{argmin}} \mathbb{E}_{x, y \sim D_{\text{train}}} [\mathcal{L}_{\text{NCE}}(x, y, \theta; \mathcal{S})] \tag{11}$$

Here, we showed that the vanilla contrastive loss function, Equation 8, serves as a surrogate objective for optimizing our desired invariance objective, Equation 9. By incorporating contrastive learning alongside the maximum likelihood objective in Equation 6, ILO effectively reveals the underlying invariances in the pruned model.

Additional Discussion on Lazy Training

The lazy training regime (Chizat, Oyallon, and Bach 2019; Tzen and Raginsky 2020) is a phenomenon when loss rapidly decreases, while weight values stay relatively constant. This phenomenon occurs on large over-parameterized neural networks (Chizat, Oyallon, and Bach 2019). Because the weight values stay relatively constant, the magnitude ordering between weights also changes very little. Therefore, network pruning struggles to preserve such loss decreases in the lazy training regime (Liu et al. 2023).

Because weights with very small magnitude have minimal effect on the output logits, pruning said weights will not drastically hurt performance. Thus, if the pruning framework can separate very small magnitude weights from normal weights prior to the lazy training regime, we can preserve loss decreases in the lazy training regime. The PIS setting accomplishes this by initializing all weights to be very small so that only important weights will learn large magnitudes. This guarantees that a large percentage of weights will

Dataset	$g(\cdot)$	MLP _{vis}	IUNET ^(MLP_{vis})
CIFAR10	resize.	44.096 ± 0.434	97.349 ± 4.590
	horiz.	80.485 ± 0.504	99.413 ± 1.016
	color.	56.075 ± 0.433	98.233 ± 3.060
	grayscale.	81.932 ± 0.233	99.077 ± 1.598
CIFAR100	resize.	32.990 ± 1.065	39.936 ± 2.786
	horiz.	70.793 ± 0.677	77.935 ± 1.464
	color.	31.704 ± 0.560	51.397 ± 2.709
	grayscale.	71.245 ± 0.467	76.476 ± 1.245
SVHN	resize.	36.708 ± 2.033	77.440 ± 0.627
	horiz.	71.400 ± 1.651	95.082 ± 0.166
	color.	61.341 ± 0.946	91.097 ± 0.395
	grayscale.	90.344 ± 0.233	99.259 ± 0.073

Table 6: Comparing the consistency metric (%) of the untrained supernet, MLP_{vis} and MLP_{TAB}, against IUNET’s pruned subnetwork under different invariant transforms, $g(\cdot)$. IUNET preserves invariances better.

have small magnitudes throughout training, while important larger magnitude weights will emerge over the course of training.

Additional Experiments

Effects of Proactive Initialization: Full Results

We provide weight histograms on CIFAR100 and SVHN in Figure 5. As shown, the trends reported in the main text holds on other datasets.

On Weight Visualization: Full Results

We provide weight visualizations on CIFAR100 and SVHN in Figure 6. As shown, the trends reported in the main text holds on other datasets.

On Consistency: Full Results

We provide consistency experiments on CIFAR100 and SVHN in Table 6. As shown, the trends reported in the main text holds on other datasets.

Implementation Details

Dataset Details

We considered the following *computer vision* datasets: CIFAR10, CIFAR100 (Krizhevsky, Hinton et al. 2009), and SVHN (Netzer et al. 2011). CIFAR10 and CIFAR100 are multi-domain image classification datasets. SVHN is a street sign digit classification dataset. Input images are 32×32 color images. We split the train set by 80/20 for training and validation. We test on the test set provided separately. We reported dataset statistics in Table 7.

We considered 40 tabular datasets from OpenML (Gijbbers et al. 2019), UCI (Asuncion and Newman 2007), and Kaggle, following the MLP_{TAB+C} benchmark (Kadra et al. 2021). These tabular datasets cover a variety of domains, data types, and class imbalances. We used a 60/20/20 train validation test split, and reported dataset statistics in Table 8. We use a random seed of 11 for the data split, following prior work (Kadra et al. 2021).

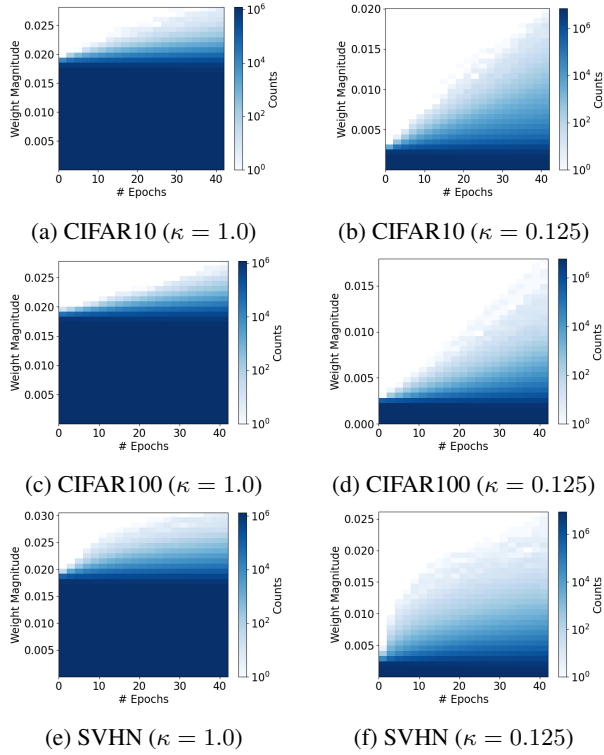


Figure 5: Histogram of weight magnitudes, $|\theta_M^{(t)}|$, plotted over each epoch under different κ initializations settings. $\kappa = 1.0$ means normal initialization. Results shown for MLP_{VIS} on the CIFAR10, CIFAR100, and SVHN datasets.

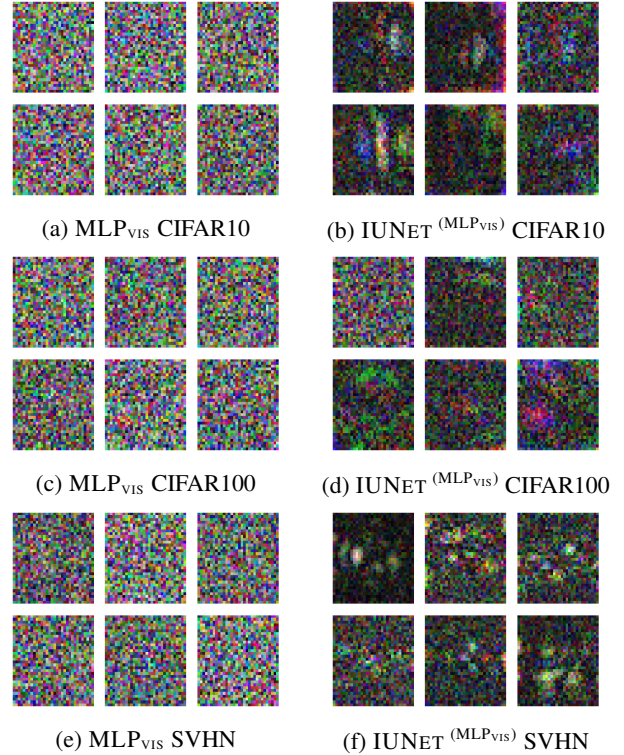


Figure 6: Visualization of weight magnitudes, $|\theta_M^{(T)}|$, trained with different policies. The models were trained on CIFAR10, CIFAR100, and SVHN. The magnitude of each RGB pixel for 6 output logits are plotted.

Hyperparameter Settings

All experiments were run 3 times from scratch starting with different random seeds. We report both the mean and standard deviation of all runs. All hyperparameters were chosen based on validation set results.

For all experiments, we used $\lambda = 1$, which was chosen through a grid search over $\lambda \in \{0.25, 0.5, 1.0\}$. For all experiments, we used a batch size of 128. For pre-pruning training, we used SGD with Nesterov momentum and a learning rate of 0.001, following past works (Blalock et al. 2020). For finetuning vision datasets, we used the same optimizer setup except with 16-bit operations except for batch normalization, following β -LASSO (Neyshabur 2020). For finetuning tabular datasets, we used AdamW (Loshchilov and Hutter 2017), a learning rate of 0.001s, decoupled weight decay, cosine annealing with restart, initial restart budget of 15 epochs, budget multiplier of 2, and snapshot ensembling (Huang et al. 2017), following prior works (Kadra et al. 2021; Zimmer, Lindauer, and Hutter 2021). It is important to note we did not tune the dataset and training hyperparameters for each tabular dataset individually like $\text{MLP}_{\text{TAB+C}}$ (Kadra et al. 2021), rather taking the most effective setting on average.

For tabular datasets, we tuned the compression ratio over the following range of values: $r \in \{2, 4, 8\}$ and the PIs multiplier over the following range of values: $\kappa \in \{0.25, 0.125, 0.0625\}$, on a subset of 4 tabular datasets. We found that $r = 8$ and $\kappa = 0.25$ performs the most consistently and used this setting for all runs of IUNET in the main paper. It is important to note we did not tune hyperparameters for IUNET on each individual tabular dataset like $\text{MLP}_{\text{TAB+C}}$ (Kadra et al. 2021), making IUNET a much more efficient model than $\text{MLP}_{\text{TAB+C}}$. For the tabular baselines (Chen and Guestrin 2016; Arik and Pfister 2021; Kadra et al. 2021), we used the same hyperparameter tuning setup as the MLP+C benchmark (Kadra et al. 2021).

For vision datasets, we tuned the compression ratio over the following range of values: $r \in \{2, 4, 8, 16\}$ on each individual dataset for all network pruning models except β -LASSO⁴. For β -lasso (Neyshabur 2020), we tuned the hyperparameters over the range $\beta = \{50\}$ and L1 regularization in $l1 \in \{10^{-6}, 2 \times 10^{-6}, 5 \times 10^{-6}, 10^{-5}, 2 \times 10^{-5}\}$ on each individual dataset as done in the original paper. It is important to note that although we tuned both hyperparameters for both IUNET and baselines on each individual datasets, our main and ablation table rankings stay consistent had we chosen a single setting for all datasets, as shown in the detailed pruning experiments in the main paper.

Supernetwork Architecture

MLP_{VIS} is a deep MLP that contains a CNN subnetwork. Given a scaling factor, α , the CNN architecture consists of 3x3 convolutional layers with the following (out channels, stride) settings: $[(\alpha, 1), (2\alpha, 2), (2\alpha, 1), (4\alpha, 2), (4\alpha, 1), (8\alpha, 2), (8\alpha, 1), (16\alpha, 2)]$ followed by a hidden layer of dimension 64α . It is worth noting that our CNN does

⁴This is because β -LASSO does not accept a chosen compression ratio as a hyperparameter.

not include maxpooling layers for fair comparison with the learned architectures, following the same setup as β -LASSO (Neyshabur 2020). To form the MLP Network, we ensured the CNN network structure exists as a subnetwork within the MLP supernetwork by setting the hidden layer sizes to: $[\alpha s^2, \frac{\alpha s^2}{2}, \frac{\alpha s^2}{2}, \frac{\alpha s^2}{4}, \frac{\alpha s^2}{4}, \frac{\alpha s^2}{8}, \frac{\alpha s^2}{8}, \frac{\alpha s^2}{16}, 64\alpha]$. This architecture was also introduced in β -Lasso (Neyshabur 2020). All layers are preceded by batch normalization and ReLU activation. We chose $\alpha = 8$ such that our supernetwork can fit onto an Nvidia RTX 3070 GPU.

CNN is the corresponding CNN subnetwork with (out channels, stride) settings: $[(\alpha, 1), (2\alpha, 2), (2\alpha, 1), (4\alpha, 2), (4\alpha, 1), (8\alpha, 2), (8\alpha, 1), (16\alpha, 2)]$, derived from prior works (Neyshabur 2020). Again, we chose $\alpha = 8$ to be consistent with MLP_{VIS} .

RESNET (He et al. 2016) is the standard RESNET-18 model used in past benchmarks (Blalock et al. 2020). Resnet differs from CNN in its inclusion of max-pooling layers and residual connections.

MLP_{TAB} is a 9-layer MLP with hidden dimension 512, batch normalization, and ReLU activation. We did not use dropout or skip connections as it was found to be ineffective on most tabular datasets in MLP+C (Kadra et al. 2021).

Pruning Implementation Details

Following Shrinkbench (Blalock et al. 2020), we use magnitude-based pruning only on the encoder, $f_{\mathcal{E}}$, keeping all weights in the decoder, $f_{\mathcal{D}}$. This is done to prevent pruning a cutset in the decoder architecture, so that all class logits receive input signal. To optimize the performance, we apply magnitude-based pruning globally, instead of layer-wise.

Hardware

All experiments were conducted on an Nvidia V100 GPU and an AMD EPYC 7402 CPU. The duration of the tabular experiments varied, ranging from a few minutes up to half a day, depending on the specific dataset-model pair and the training phase (pre-pruning training or finetuning). For the vision experiments, a single setting on a single dataset-model pair required a few hours for both pre-pruning training and finetuning.

References

- Arik, S. Ö.; and Pfister, T. 2021. Tabnet: Attentive interpretable tabular learning. In *Proceedings of the AAAI conference on artificial intelligence*, volume 35, 6679–6687.
- Arpit, D.; Jastrzębski, S.; Ballas, N.; Krueger, D.; Bengio, E.; Kanwal, M. S.; Maharaj, T.; Fischer, A.; Courville, A.; Bengio, Y.; et al. 2017. A closer look at memorization in deep networks. In *International conference on machine learning*, 233–242. PMLR.
- Asuncion, A.; and Newman, D. 2007. UCI machine learning repository.
- Baevski, A.; Zhou, Y.; Mohamed, A.; and Auli, M. 2020. wav2vec 2.0: A framework for self-supervised learning of speech representations. *Advances in neural information processing systems*, 33: 12449–12460.

Dataset	# Train Instances	# Valid Instances	# Test Instances	Number of Classes
CIFAR10	40000	10000	10000	10
CIFAR100	40000	10000	10000	100
SVHN	58606	14651	26032	10

Table 7: Statistics on computer vision datasets.

Dataset	# Train Inst.	# Valid Inst.	# Test Inst.	# Feats.	Majority Class %	Minority Class %	OpenML ID
Anneal	538	179	179	39	76.17	0.89	233090
Kr-vs-kp	1917	639	639	37	52.22	47.78	233091
Arrhythmia	271	90	90	280	54.20	0.44	233092
Mfeat-factors	1200	400	400	217	10.00	10.00	233093
Credit-g	600	200	200	21	70.00	30.00	233088
Vehicle	507	169	169	19	25.77	23.52	233094
Kc1	1265	421	421	22	84.54	15.46	233096
Adult	29305	9768	9768	15	76.07	23.93	233099
Walking-activity	89599	29866	29866	5	14.73	0.61	233102
Phoneme	3242	1080	1080	6	70.65	29.35	233103
Skin-segmentation	147034	49011	49011	4	79.25	20.75	233104
Ldpa	98916	32972	32972	8	33.05	0.84	233106
Nomao	20679	6893	6893	119	71.44	28.56	233107
Cnae-9	648	216	216	857	11.11	11.11	233108
Blood-transfusion	448	149	149	5	76.20	23.80	233109
Bank-marketing	27126	9042	9042	17	88.30	11.70	233110
Connect-4	40534	13511	13511	43	65.83	9.55	233112
Shuttle	34800	11600	11600	10	78.60	0.02	233113
Higgs	58830	19610	19610	29	52.86	47.14	233114
Australian	414	138	138	15	55.51	44.49	233115
Car	1036	345	345	7	70.02	3.76	233116
Segment	1386	462	462	20	14.29	14.29	233117
Fashion-MNIST	42000	14000	14000	785	10.00	10.00	233118
Jungle-Chess-2pcs	26891	8963	8963	7	51.46	9.67	233119
Numerai28.6	57792	19264	19264	22	50.52	49.48	233120
Devnagari-Script	55200	18400	18400	1025	2.17	2.17	233121
Helena	39117	13039	13039	28	6.14	0.17	233122
Jannis	50239	16746	16746	55	46.01	2.01	233123
Volkert	34986	11662	11662	181	21.96	2.33	233124
MiniBooNE	78038	26012	26012	51	71.94	28.06	233126
APSFailure	45600	15200	15200	171	98.19	1.81	233130
Christine	3250	1083	1083	1637	50.00	50.00	233131
Dilbert	6000	2000	2000	2001	20.49	19.13	233132
Fabert	4942	1647	1647	801	23.39	6.09	233133
Jasmine	1790	596	596	145	50.00	50.00	233134
Sylvine	3074	1024	1024	21	50.00	50.00	233135
Dionis	249712	83237	83237	61	0.59	0.21	233137
Aloi	64800	21600	21600	129	0.10	0.10	233142
C.C.FraudD	170884	56961	56961	31	99.83	0.17	233143
Click Prediction	239689	79896	79896	12	83.21	16.79	233146

Table 8: Statistics on tabular datasets. Note that the OpenML ID denotes the ID used to retrieve the dataset (Gijbbers et al. 2019). Majority and Minority Class % shows the class imbalance within each dataset. For fair evaluation, we report balanced accuracy in all tabular experiments. # Feats. denotes the number of features in each dataset.

- Bahri, D.; Jiang, H.; Tay, Y.; and Metzler, D. 2021. Scarf: Self-supervised contrastive learning using random feature corruption. *arXiv preprint arXiv:2106.15147*.
- Benton, G.; Finzi, M.; Izmailov, P.; and Wilson, A. G. 2020. Learning invariances in neural networks from training data. *Advances in neural information processing systems*, 33: 17605–17616.
- Blalock, D.; Gonzalez Ortiz, J. J.; Frankle, J.; and Gutttag, J. 2020. What is the state of neural network pruning? *Proceedings of machine learning and systems*, 2: 129–146.
- Borisov, V.; Leemann, T.; Seßler, K.; Haug, J.; Pawelczyk, M.; and Kasneci, G. 2022. Deep neural networks and tabular data: A survey. *IEEE Transactions on Neural Networks and Learning Systems*.
- Bronstein, M. M.; Bruna, J.; LeCun, Y.; Szlam, A.; and Vandergheynst, P. 2017. Geometric deep learning: going beyond euclidean data. *IEEE Signal Processing Magazine*, 34(4): 18–42.
- Chen, T.; and Guestrin, C. 2016. Xgboost: A scalable tree boosting system. In *Proceedings of the 22nd acm sigkdd international conference on knowledge discovery and data mining*, 785–794.
- Chen, T.; Kornblith, S.; Norouzi, M.; and Hinton, G. 2020. A simple framework for contrastive learning of visual representations. In *International conference on machine learning*, 1597–1607. PMLR.
- Chen, X.; Xie, S.; and He, K. 2021. An empirical study of training self-supervised vision transformers. In *Proceedings of the IEEE/CVF International Conference on Computer Vision*, 9640–9649.
- Chizat, L.; Oyallon, E.; and Bach, F. 2019. On lazy training in differentiable programming. *Advances in neural information processing systems*, 32.
- Chopra, S.; Hadsell, R.; and LeCun, Y. 2005. Learning a similarity metric discriminatively, with application to face verification. In *2005 IEEE Computer Society Conference on Computer Vision and Pattern Recognition (CVPR'05)*, volume 1, 539–546. IEEE.
- Cohen, T.; and Welling, M. 2016. Group equivariant convolutional networks. In *International conference on machine learning*, 2990–2999. PMLR.
- Corti, F.; Entezari, R.; Hooker, S.; Bacciu, D.; and Saukh, O. 2022. Studying the impact of magnitude pruning on contrastive learning methods. *arXiv preprint arXiv:2207.00200*.
- Cubuk, E. D.; Zoph, B.; Mane, D.; Vasudevan, V.; and Le, Q. V. 2018. Autoaugment: Learning augmentation policies from data. *arXiv preprint arXiv:1805.09501*.
- Cybenko, G. 1989. Approximation by superpositions of a sigmoidal function. *Mathematics of control, signals and systems*, 2(4): 303–314.
- Dangovski, R.; Jing, L.; Loh, C.; Han, S.; Srivastava, A.; Cheung, B.; Agrawal, P.; and Soljačić, M. 2021. Equivariant contrastive learning. *arXiv preprint arXiv:2111.00899*.
- Defferrard, M.; Bresson, X.; and Vandergheynst, P. 2016. Convolutional neural networks on graphs with fast localized spectral filtering. *Advances in neural information processing systems*, 29.
- Dehmamy, N.; Walters, R.; Liu, Y.; Wang, D.; and Yu, R. 2021. Automatic symmetry discovery with lie algebra convolutional network. *Advances in Neural Information Processing Systems*, 34: 2503–2515.
- Delchevalerie, V.; Bibal, A.; Frénay, B.; and Mayer, A. 2021. Achieving rotational invariance with bessel-convolutional neural networks. *Advances in Neural Information Processing Systems*, 34: 28772–28783.
- Deng, C.; Litany, O.; Duan, Y.; Poulencard, A.; Tagliasacchi, A.; and Guibas, L. J. 2021. Vector neurons: A general framework for so(3)-equivariant networks. In *Proceedings of the IEEE/CVF International Conference on Computer Vision*, 12200–12209.
- Evcı, U.; Gale, T.; Menick, J.; Castro, P. S.; and Elsen, E. 2020. Rigging the lottery: Making all tickets winners. In *International Conference on Machine Learning*, 2943–2952. PMLR.
- Frankle, J.; and Carbin, M. 2018. The lottery ticket hypothesis: Finding sparse, trainable neural networks. *arXiv preprint arXiv:1803.03635*.
- Gijsbers, P.; LeDell, E.; Thomas, J.; Poirier, S.; Bischl, B.; and Vanschoren, J. 2019. An open source AutoML benchmark. *arXiv preprint arXiv:1907.00909*.
- Glorot, X.; and Bengio, Y. 2010. Understanding the difficulty of training deep feedforward neural networks. In *Proceedings of the thirteenth international conference on artificial intelligence and statistics*, 249–256. JMLR Workshop and Conference Proceedings.
- Gorishniy, Y.; Rubachev, I.; and Babenko, A. 2022. On embeddings for numerical features in tabular deep learning. *Advances in Neural Information Processing Systems*, 35: 24991–25004.
- Gorishniy, Y.; Rubachev, I.; Khrulkov, V.; and Babenko, A. 2021. Revisiting deep learning models for tabular data. *Advances in Neural Information Processing Systems*, 34: 18932–18943.
- Grinsztajn, L.; Oyallon, E.; and Varoquaux, G. 2022. Why do tree-based models still outperform deep learning on tabular data? *arXiv preprint arXiv:2207.08815*.
- He, K.; Zhang, X.; Ren, S.; and Sun, J. 2015. Delving deep into rectifiers: Surpassing human-level performance on imagenet classification. In *Proceedings of the IEEE international conference on computer vision*, 1026–1034.
- He, K.; Zhang, X.; Ren, S.; and Sun, J. 2016. Deep residual learning for image recognition. In *Proceedings of the IEEE conference on computer vision and pattern recognition*, 770–778.
- Hoang, D. N.; Liu, S.; Marculescu, R.; and Wang, Z. 2023. REVISITING PRUNING AT INITIALIZATION THROUGH THE LENS OF RAMANUJAN GRAPH. In *The Eleventh International Conference on Learning Representations*.

- Hollmann, N.; Müller, S.; Eggenberger, K.; and Hutter, F. 2022. TabPFN: A transformer that solves small tabular classification problems in a second. *arXiv preprint arXiv:2207.01848*.
- Huang, G.; Li, Y.; Pleiss, G.; Liu, Z.; Hopcroft, J. E.; and Weinberger, K. Q. 2017. Snapshot ensembles: Train 1, get m for free. *arXiv preprint arXiv:1704.00109*.
- Huang, X.; Khetan, A.; Cvitkovic, M.; and Karnin, Z. 2020. Tabtransformer: Tabular data modeling using contextual embeddings. *arXiv preprint arXiv:2012.06678*.
- Immer, A.; van der Ouderaa, T.; Rätsch, G.; Fortuin, V.; and van der Wilk, M. 2022. Invariance learning in deep neural networks with differentiable Laplace approximations. *Advances in Neural Information Processing Systems*, 35: 12449–12463.
- Jaderberg, M.; Simonyan, K.; Zisserman, A.; et al. 2015. Spatial transformer networks. *Advances in neural information processing systems*, 28.
- Jaiswal, A.; Babu, A. R.; Zadeh, M. Z.; Banerjee, D.; and Makedon, F. 2020. A survey on contrastive self-supervised learning. *Technologies*, 9(1): 2.
- Joseph, M.; and Raj, H. 2022. GATE: Gated Additive Tree Ensemble for Tabular Classification and Regression. *arXiv preprint arXiv:2207.08548*.
- Kadra, A.; Lindauer, M.; Hutter, F.; and Grabocka, J. 2021. Well-tuned simple nets excel on tabular datasets. *Advances in neural information processing systems*, 34: 23928–23941.
- Kipf, T. N.; and Welling, M. 2016. Semi-supervised classification with graph convolutional networks. *arXiv preprint arXiv:1609.02907*.
- Kirsch, L.; Flennerhag, S.; van Hasselt, H.; Friesen, A.; Oh, J.; and Chen, Y. 2022. Introducing symmetries to black box meta reinforcement learning. In *Proceedings of the AAAI Conference on Artificial Intelligence*, volume 36, 7202–7210.
- Krizhevsky, A.; Hinton, G.; et al. 2009. Learning multiple layers of features from tiny images.
- LeCun, Y.; Bengio, Y.; and Hinton, G. 2015. Deep learning. *nature*, 521(7553): 436–444.
- LeCun, Y.; Bottou, L.; Bengio, Y.; and Haffner, P. 1998. Gradient-based learning applied to document recognition. *Proceedings of the IEEE*, 86(11): 2278–2324.
- Lee, N.; Ajanthan, T.; Gould, S.; and Torr, P. H. 2019. A signal propagation perspective for pruning neural networks at initialization. *arXiv preprint arXiv:1906.06307*.
- Liu, H.; Simonyan, K.; and Yang, Y. 2018. Darts: Differentiable architecture search. *arXiv preprint arXiv:1806.09055*.
- Liu, S.; Chen, T.; Zhang, Z.; Chen, X.; Huang, T.; Jaiswal, A.; and Wang, Z. 2023. Sparsity May Cry: Let Us Fail (Current) Sparse Neural Networks Together! *arXiv preprint arXiv:2303.02141*.
- Liu, Z.; Sun, M.; Zhou, T.; Huang, G.; and Darrell, T. 2018. Rethinking the value of network pruning. *arXiv preprint arXiv:1810.05270*.
- Lorraine, J.; Vicol, P.; and Duvenaud, D. 2020. Optimizing millions of hyperparameters by implicit differentiation. In *International Conference on Artificial Intelligence and Statistics*, 1540–1552. PMLR.
- Loshchilov, I.; and Hutter, F. 2017. Decoupled weight decay regularization. *arXiv preprint arXiv:1711.05101*.
- Louizos, C.; Welling, M.; and Kingma, D. P. 2017. Learning sparse neural networks through L_0 regularization. *arXiv preprint arXiv:1712.01312*.
- Luo, R.; Tian, F.; Qin, T.; Chen, E.; and Liu, T.-Y. 2018. Neural architecture optimization. *Advances in neural information processing systems*, 31.
- Ma, X.; Yuan, G.; Shen, X.; Chen, T.; Chen, X.; Chen, X.; Liu, N.; Qin, M.; Liu, S.; Wang, Z.; et al. 2021. Sanity checks for lottery tickets: Does your winning ticket really win the jackpot? *Advances in Neural Information Processing Systems*, 34: 12749–12760.
- Netzer, Y.; Wang, T.; Coates, A.; Bissacco, A.; Wu, B.; and Ng, A. Y. 2011. Reading digits in natural images with unsupervised feature learning.
- Neyshabur, B. 2017. Implicit regularization in deep learning. *arXiv preprint arXiv:1709.01953*.
- Neyshabur, B. 2020. Towards learning convolutions from scratch. *Advances in Neural Information Processing Systems*, 33: 8078–8088.
- Neyshabur, B.; Tomioka, R.; and Srebro, N. 2014. In search of the real inductive bias: On the role of implicit regularization in deep learning. *arXiv preprint arXiv:1412.6614*.
- Oh Song, H.; Xiang, Y.; Jegelka, S.; and Savarese, S. 2016. Deep metric learning via lifted structured feature embedding. In *Proceedings of the IEEE conference on computer vision and pattern recognition*, 4004–4012.
- Pasad, A.; Chou, J.-C.; and Livescu, K. 2021. Layer-wise analysis of a self-supervised speech representation model. In *2021 IEEE Automatic Speech Recognition and Understanding Workshop (ASRU)*, 914–921. IEEE.
- Pham, H.; Guan, M.; Zoph, B.; Le, Q.; and Dean, J. 2018. Efficient neural architecture search via parameters sharing. In *International conference on machine learning*, 4095–4104. PMLR.
- Popov, S.; Morozov, S.; and Babenko, A. 2019. Neural oblivious decision ensembles for deep learning on tabular data. *arXiv preprint arXiv:1909.06312*.
- Qi, C. R.; Yi, L.; Su, H.; and Guibas, L. J. 2017. Pointnet++: Deep hierarchical feature learning on point sets in a metric space. *Advances in neural information processing systems*, 30.
- Quiroga, F.; Ronchetti, F.; Lanzarini, L.; and Bariviera, A. F. 2020. Revisiting data augmentation for rotational invariance in convolutional neural networks. In *Modelling and Simulation in Management Sciences: Proceedings of the International Conference on Modelling and Simulation in Management Sciences (MS-18)*, 127–141. Springer.
- Sabour, S.; Frosst, N.; and Hinton, G. E. 2017. Dynamic routing between capsules. *Advances in neural information processing systems*, 30.

- Satorras, V. G.; Hoogeboom, E.; and Welling, M. 2021. E(n) equivariant graph neural networks. In *International conference on machine learning*, 9323–9332. PMLR.
- Schäfl, B.; Gruber, L.; Bitto-Nemling, A.; and Hochreiter, S. 2022. Hopular: Modern Hopfield Networks for Tabular Data. *arXiv preprint arXiv:2206.00664*.
- Schroff, F.; Kalenichenko, D.; and Philbin, J. 2015. Facenet: A unified embedding for face recognition and clustering. In *Proceedings of the IEEE conference on computer vision and pattern recognition*, 815–823.
- Shwartz-Ziv, R.; and Armon, A. 2022. Tabular data: Deep learning is not all you need. *Information Fusion*, 81: 84–90.
- Singla, V.; Ge, S.; Ronen, B.; and Jacobs, D. 2021. Shift invariance can reduce adversarial robustness. *Advances in Neural Information Processing Systems*, 34: 1858–1871.
- Tolstikhin, I. O.; Houlsby, N.; Kolesnikov, A.; Beyer, L.; Zhai, X.; Unterthiner, T.; Yung, J.; Steiner, A.; Keysers, D.; Uszkoreit, J.; et al. 2021. Mlp-mixer: An all-mlp architecture for vision. *Advances in neural information processing systems*, 34: 24261–24272.
- Tzen, B.; and Raginsky, M. 2020. A mean-field theory of lazy training in two-layer neural nets: entropic regularization and controlled McKean-Vlasov dynamics. *arXiv preprint arXiv:2002.01987*.
- Vaswani, A.; Shazeer, N.; Parmar, N.; Uszkoreit, J.; Jones, L.; Gomez, A. N.; Kaiser, Ł.; and Polosukhin, I. 2017. Attention is all you need. *Advances in neural information processing systems*, 30.
- Wan, A.; Dai, X.; Zhang, P.; He, Z.; Tian, Y.; Xie, S.; Wu, B.; Yu, M.; Xu, T.; Chen, K.; et al. 2020. Fbnetv2: Differentiable neural architecture search for spatial and channel dimensions. In *Proceedings of the IEEE/CVF Conference on Computer Vision and Pattern Recognition*, 12965–12974.
- Wang, C.; Zhang, G.; and Grosse, R. 2020. Picking winning tickets before training by preserving gradient flow. *arXiv preprint arXiv:2002.07376*.
- Wu, Z.; Pan, S.; Chen, F.; Long, G.; Zhang, C.; and Philip, S. Y. 2020. A comprehensive survey on graph neural networks. *IEEE transactions on neural networks and learning systems*, 32(1): 4–24.
- Xie, S.; Kirillov, A.; Girshick, R.; and He, K. 2019. Exploring randomly wired neural networks for image recognition. In *Proceedings of the IEEE/CVF International Conference on Computer Vision*, 1284–1293.
- Xu, Y.; Xiao, T.; Zhang, J.; Yang, K.; and Zhang, Z. 2014. Scale-invariant convolutional neural networks. *arXiv preprint arXiv:1411.6369*.
- You, J.; Leskovec, J.; He, K.; and Xie, S. 2020a. Graph structure of neural networks. In *International Conference on Machine Learning*, 10881–10891. PMLR.
- You, Y.; Chen, T.; Sui, Y.; Chen, T.; Wang, Z.; and Shen, Y. 2020b. Graph contrastive learning with augmentations. *Advances in neural information processing systems*, 33: 5812–5823.
- Zhang, C.; Bengio, S.; Hardt, M.; Recht, B.; and Vinyals, O. 2021. Understanding deep learning (still) requires rethinking generalization. *Communications of the ACM*, 64(3): 107–115.
- Zhou, A.; Knowles, T.; and Finn, C. 2020. Meta-learning symmetries by reparameterization. *arXiv preprint arXiv:2007.02933*.
- Zhu, Y.; Xu, Y.; Yu, F.; Liu, Q.; Wu, S.; and Wang, L. 2021. Graph contrastive learning with adaptive augmentation. In *Proceedings of the Web Conference 2021*, 2069–2080.
- Zimmer, L.; Lindauer, M.; and Hutter, F. 2021. Auto-pytorch: Multi-fidelity metalearning for efficient and robust autodl. *IEEE Transactions on Pattern Analysis and Machine Intelligence*, 43(9): 3079–3090.
- Zoph, B.; Vasudevan, V.; Shlens, J.; and Le, Q. V. 2018. Learning transferable architectures for scalable image recognition. In *Proceedings of the IEEE conference on computer vision and pattern recognition*, 8697–8710.